A Compact Active Ka-Band Filtenna for CubeSats

Marios Patriotis, Firas N. Ayoub, Youssef Tawk, *Senior Member, IEEE*, Joseph Costantine, *Senior Member, IEEE*, and Christos G. Christodoulou, *Life Fellow, IEEE*

***Abstract*—This letter describes the design of a right-hand circularly polarized planar filtenna (filter + antenna) that can reconfigure its operation between two center frequencies in the Ka-band. The filtenna structure is composed of a four-element array radiator and a reconfigurable bandpass filter, occupying an area of 31 × 14 mm. The circularly polarized array elements are fed by a sequential power divider for an enhanced polarization purity. The filter is based on a ring resonator loaded with a variable open stub. The length of the stub extends through a p-i-n diode switch, resulting in a change of the loaded reactance into the ring, and consequently tuning the filter's operating center frequency from 30.3 to 29 GHz. The proposed low-loss filtenna structure exhibits a reconfigurable fractional bandwidth up to 7.74%, a peak realized gain that can reach up to 11.5 dBic, an axial ratio of less than 1 dB, and a sidelobe level that can go as low as −12 dB. The prototype filtenna is fabricated and tested, where the measured results verify the simulated data. A figure of merit is proposed to highlight the superior performance of the presented Ka-band structure in terms of the polarization, size, reconfiguration ability, and radiation characteristics as proven by the comparison with other works in the literature.**

***Index Terms*—Bandpass filter (BPF), CubeSat antenna, filtenna, Ka-band, reconfigurable filter, reconfigurable frequency, ring resonator.**

I. Introduction

The use of nanosatellite (CubeSat) clusters is cost effective and meets new space communication requirements. Hence, CubeSats are rapidly deployed in orbit, causing a congested RF environment and an increased information exchange between the satellite units in space. Moreover, satellite communication links require high data rates without interference from nearby CubeSats. This can be addressed with the design of wider bandwidth planar printed reconfigurable communication systems in the Ka-band [1]–[3].

Frequency reconfiguration of an antenna is possible by either altering the electromagnetic coupling environment of the antenna or by changing the antenna shape itself [4]–[11]. For example, in [8], parasitic elements are manually placed at an optimized distance from the radiator to create capacitance loading, resulting in a change in the antenna bandwidth. The lack of an automated mechanism makes the model impractical for CubeSats. In [9], an antenna patch resides on a liquid crystal-filled cavity biased by a 20 V voltage source. The difficulty of constraining the liquid in a cavity and the high-voltage potential needed for the proper antenna functioning makes it an unattractive candidate for space operations. In [10], a slotted waveguide antenna accommodates optical switches over the slots to reduce their size when those are activated and accordingly cause frequency reconfiguration. Such a model requires an increased number of active components and photo emitters. In [11], a fractal-type antenna is resized by numerous p-i-n switches that connect metallic sections in order to reconfigure its operation.

On the other hand, the combination of a reconfigurable bandpass filter (BPF) and an antenna array component forms the so-called active filtenna structure. Such integration achieves frequency reconfiguration. Active filtenna models are suggested mainly in frequencies below 10 GHz [12]–[18]. For instance, in [14], two resonating structures are incorporated in the antenna feeding network in order to tune the operating frequency in the C-band. In [17], a resonating structure is proposed for potential frequency tuning at the K-band.

In fact, the design of reconfigurable antennas to operate in the Ka-band is a challenging task due to the scarcity of the available active components and the sensitivity of the design requirements. In addition, passive elements for the dc biasing of the integrated active components are either unavailable or suffer from a narrow dynamic range. Moreover, the fabrication of active antennas at the Ka-band can be taxing due to the small dimensions and the need to reduce any unnecessary losses.

While the sequentially fed circularly polarized antenna and the filter based on a ring resonator loaded with a variable open stub may have been addressed in the literature, they have never been proposed for integration and operation at the Ka-band. Accordingly, what we present here goes beyond simply cascading these two elements. In fact, the novelty of the work is based on the full design of a dynamic filtenna structure that achieves high circular polarization (CP) purity with a reconfigurable frequency operation for the Ka-band integration.

The presented work herein, briefly introduced in [19], provides a thorough performance analysis of the Ka-band filtenna that is composed of the four-element antenna array and a reconfigurable BPF. A proposed figure of merit (FoM) proves not only the superiority of the design but also its advantageous reconfiguration ability, excellent radiation properties, and CP purity at the Ka-band.

II. Four-Element Array Antenna

The overall filtenna design is developed on a 0.5 mm thick RO3003 substrate with relative permittivity of $\varepsilon_r = 3$ and loss tangent $\tan\delta = 0.001$. The antenna array is designed to meet the

Manuscript received May 28, 2021; accepted June 23, 2021. Date of publication July 2, 2021; date of current version November 16, 2021. This work was supported by the Bluecom Systems and Consulting under Subcontract BC2016001 from Phase II NASA STTR under Contract NNX17CC01C. *(Corresponding author: Joseph Costantine.)*

Marios Patriotis, Firas N. Ayoub, and Christos G. Christodoulou are with the Electrical and Computer Engineering Department, University of New Mexico, Albuquerque, NM 87131 USA (e-mail: patriotis.marios@gmail.com; fayoub00@unm.edu; christos@unm.edu).

Youssef Tawk and Joseph Costantine are with the Electrical and Computer Engineering Department, American University of Beirut, Beirut 1107 2020, Lebanon (e-mail: yatawk@ieee.org; jcostantine@ieee.org).

Digital Object Identifier 10.1109/LAWP.2021.3094276

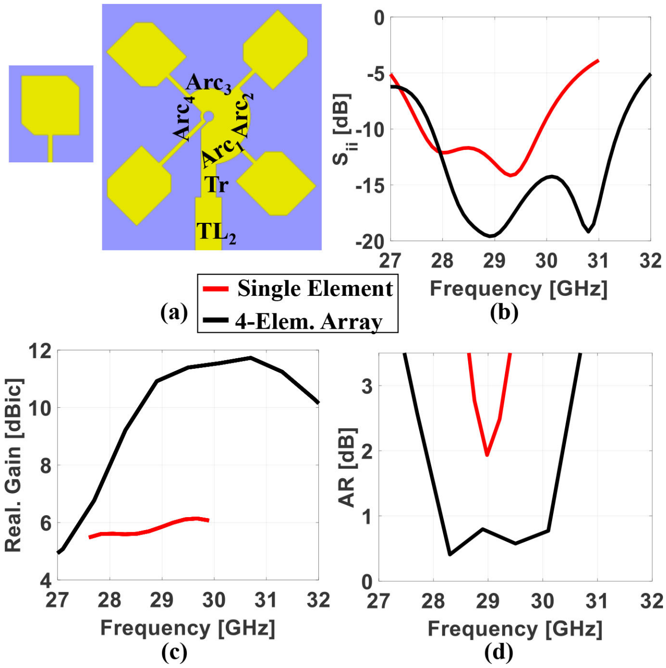

Fig. 1. (a) Four-element antenna array. (b) Performance of the single-element and four-element arrays in terms of the reflection coefficient. (c) RHCP gain. (d) AR [dB].

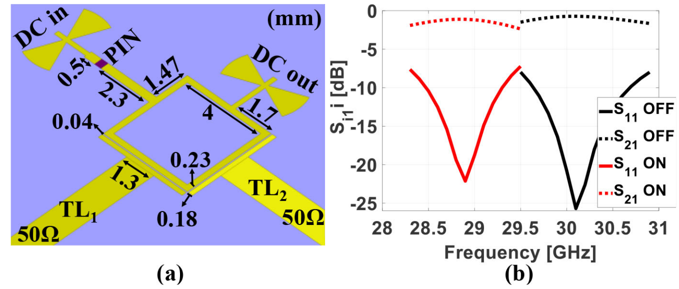

Fig. 2. (a) Detailed structure of the reconfigurable BPF. (b) Corresponding *S*-parameters' results.

required radiating characteristics by relying on a combination of CP techniques, such as truncated patches and sequential feeding network [20], [21]. The proposed array structure is shown in Fig. 1(a). Each rectangular patch has a size of 2.65×2.8 mm and a truncation length of 0.5 mm at its two opposite corners to produce the CP TM_{110} mode. In addition, this modification contributes to a larger bandwidth. The radiating elements are orthogonally cascaded to form a four-element array in a circular pattern of radius $0.3\lambda_o$. The 90° consecutively aligned radiating elements are equally power supplied with a 90° relative phase difference at 29 GHz. This is achieved by relying on a sequential power divider. Therefore, the CP condition is applied, and the AR purity is improved.

The integrated power divider consists of four arcs labeled as $\mathtt{Arc}_i$ ($i = 1$–4), as highlighted in Fig. 1(a). Each arc is connected to a 0.2 mm thick line that feeds the radiating element, whose input impedance is 125 Ω. $\mathtt{Arc}_1$ has an angular length of 45°, while $\mathtt{Arc}_{2–4}$ has an angular length of 90° each. The optimized width of each of $\mathtt{Arc}_{1–4}$ is 2.15, 2, 1.5, and 0.2 mm, respectively. At the input of the array, a microstrip line $\mathtt{TL}_2$ (50 Ω) is connected to the power divider utilizing the $\lambda_g/4$ transformer $\mathtt{TR}$ ($W = 0.75$ and $L = 1.5$ mm). The incorporation of the 50 Ω $\mathtt{TL}_2$ is essential to provide the required impedance matching when integrating the filter structure as a part of the overall proposed filtenna where the antenna array is also designed with an input impedance of 50 Ω.

The comparison in the performance between the single patch and the presented antenna array clearly shows that the proposed array configuration improves the performance in terms of the operating bandwidth [see Fig. 1(b)], right-hand circularly polarized (RHCP) gain [see Fig. 1(c)], and axial ratio (AR) [see Fig. 1(d)]. More specifically, the array design has a 3 GHz CP operating bandwidth (27.8–30.8 GHz), which is 2.4 GHz wider than the single element. Additionally, the AR at $f_c = 29$ GHz has been decreased by 1.2 dB. The RHCP gain for the operating range is now 7.2–11.65 dBic, which has been improved by 5 dBic at $f_c = 29$ GHz.

III. Reconfigurable Filter-Modified Ring Resonator

The reconfigurable BPF, developed for the active filtenna purpose, is based on a planar ring resonator circuit that is modified by loading an open stub at its side, as shown in Fig. 2(a). An RF switch (`p-i-n`) is integrated into the open stub in order to extend its length and, therefore, produces a new reactive load. The variable reactive load is the reason behind tuning the resonator's operation to a lower frequency band. Accordingly, the proposed structure relies on the least number of active components that are placed off the ring transmission line. Such a placement minimizes the insertion loss and any impedance mismatch that may be caused by the integration of the active components.

The RF switch employed for the stub length reconfiguration is the diode MA4AGP907 [22]. The activation of this switch enables the open stub of length 2.3 mm to extend by 0.35 mm, respectively. The switch circuit model used for the OFF state is a 10 kΩ resistor in parallel with a 0.02 pF capacitor, which are both connected in series to a 0.3 nH inductor ($C \| R + I$). For the switch's ON state, it is described by a 6 Ω resistor connected in series to a 0.3 nH inductor ($R + I$). The filter is initially designed for the upper band when the switch is in the OFF state. Next, the extended length of the stub is adjusted to tune the filter to a lower band when the switch is activated to the ON state.

The proposed small modification on the ring resonator provides the necessary current perturbation to achieve a significant frequency shift. The 1 GHz shift happens by utilizing only a single active component providing two operational bands, 28.5–29.3 and 29.6–30.65 GHz, as presented in Fig. 2(b) for the two respective states. The use of a single active component and its placement out of the RF current path offers reduced signal dispersion and insertion loss, with the insertion loss ranging from 0.7 to 1.7 dB for $S_{11} < -10$ dB.

A more in-depth analysis is conducted using smith chart in order to derive the equivalent loaded reactance into the ring resonator, as shown in Fig. 3. The reconfigurable filter response is recorded at the two RF switch states (OFF and ON) for the frequency range 28–31 GHz. A marker $m1$ is first placed for the matched upper band at $fc = 30.1$ GHz. Then, a second marker $m2$ is placed at the same frequency point but this time for the ON state. The respective values are used in a smith chart tool for deriving the equivalent reactance. The green curve describes the reactive load path $m1 \rightarrow m2$. Following this path results in an open stub placed

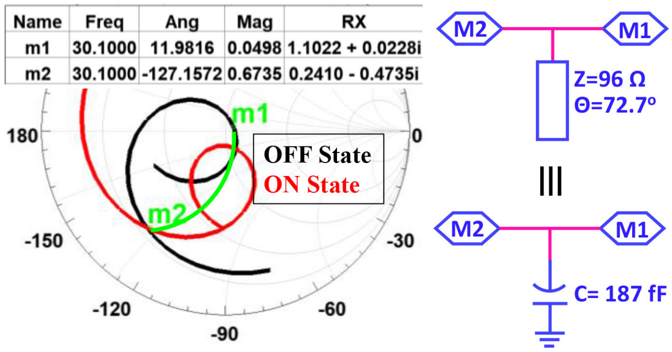

Fig. 3. Equivalent circuit of the loaded reactance into the ring resonator.

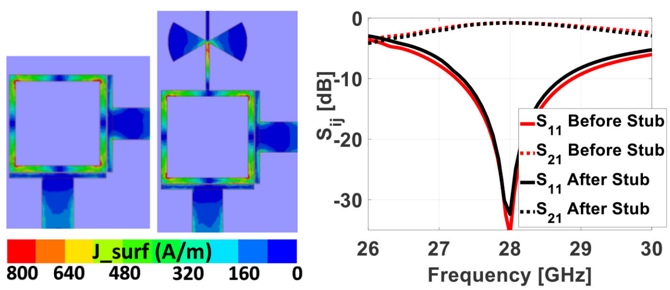

(a) (b)

Fig. 4. (a) Effect of the radial stub integration on the filter's surface current. (b) *S*-parameters' results.

in parallel with a length of 72.7° at $fc = 30.1$ GHz. The stub width of 0.35 mm is equivalent to a 96 Ω microstrip line. This modification can be described by a capacitor of 187 fF placed also in parallel.

The design of the dc bias circuitry for the activation of the RF switch is simplified by the filter configuration. The filter's ports are capacitively coupled to the ring by a small 0.04 mm gap. Such a gap enables the dc-biasing current not to leak into the filter's ports. Lumped components operating in the Ka-band are rare; accordingly, two wideband radial stubs are designed and optimized to limit the RF currents at the desired sections and also to block interferences from the dc source. As shown in Fig. 2(a), these radial stubs (dcin and dcout) are connected to the ring by employing high-impedance lines of width 0.15 mm. The objective of dcin is to supply the dc current to the diode, while dcout provides the ground connection. The radial stub dimensions (radius = 1.7 mm and angular width = 45°) and position are selected, while monitoring the current distribution on the filter and inspecting the corresponding scattering parameters. As seen in Fig. 4(a), the RF current is blocked after the stub reference point. Fig. 4(b) presents the filter's *S*-parameters before and after integrating one of the two radial stubs. For both cases, the filter behavior remains unchanged. A similar behavior is obtained after integrating the second radial stub.

IV. Active Filtenna Structure

To construct the active filtenna model, as shown in Fig. 5, the two above optimized circuits are assembled in one. The antenna array is connected to the filter's second port through a 50 Ω transmission line. Such a connection guarantees that the antenna array radiation characteristics are not altered by the layout of the filter across the various frequency bands. It is important to highlight that such a connection remains valid if the number of the array's elements is increased. Such an increase enables the filtenna to provide a higher realized gain and a further enhanced AR.

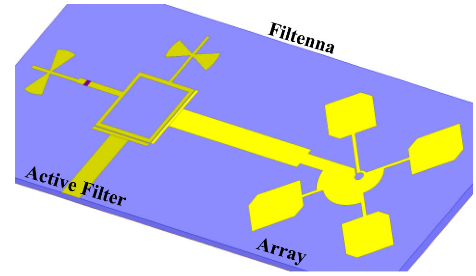

Fig. 5. Proposed reconfigurable Ka-band filtenna.

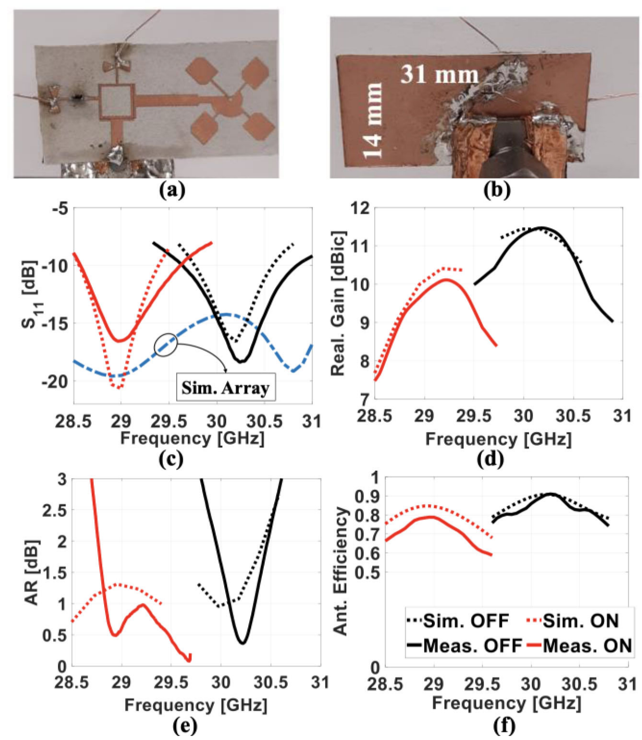

Fig. 6. (a) Top view of the fabricated prototype and (b) its corresponding bottom view. (c) Simulated and measured results of the reconfigurable filtenna array in terms of the input reflection coefficient, (d) RHCP gain, (e) AR, and (f) antenna radiation efficiency.

A prototype model for the four-element filtenna is fabricated, as seen in Fig. 6(a), using high-precision Printed Circuit Board (PCB) laser etching. For the p-i-n diode activation, a dc source of 1.5 V and 10 mA is used. Fig. 6(b) presents the bottom view of the fabricated filtenna prototype. The total filtenna structure size is 31 mm × 14 mm, while the size of a 1U CubeSat is 100 × 100 mm. Hence, this proposed structure can easily fit on one of the sides of a CubeSat. It is important to highlight that the filtenna prototype has an area that is 23 times smaller than the area of a CubeSat side in a 1U system.

The scalability of the filtenna design to various frequencies can be achieved by mainly varying the ring size of the BPF since its circumference controls the center resonant frequency. Accordingly, such frequency can be reconfigured to lower or higher bands by adjusting the reactance of the integrated shunt stub size through the integrated RF p-i-n diode switch.

TABLE I
COMPARISON WITH OTHER WORK IN THE LITERATURE

Ref.	# Rec. bands	Band	Fabric. process	Active comp.	Gain [dB]	Polarization	Voltage [V]	# Layers	Cost-Complexity	FoM
[09]	4	Ka	Printed Circuit Board	Liquid crystal	3.9	Linear	20 High	3	High	1.3
[18]	2	Ka	Lithography	Pin diode	6	Linear	1.5 Low	8	High	0.75
[23]	2	Ka	Microfabrication	RF Micro-Electromechanical Systems switch	1.74	Linear	45 High	1	High	0.87
[24]	2	W	Microfabrication	Paraffin /Heat	3	Linear	5.4 Low	6	High	0.5
[08]	2	K	Printed Circuit Board	Passive Loading /Mechanical	12	Linear	-	7	Low	3.43+
[11]	3	X, K, Ka	Printed Circuit Board	4 Pin diodes	5*	Linear	1.5x4 High	2	Low	3.75
This Work	2	Ka	Printed Circuit Board	pin diode	11.5	Circular	1.5 Low	1	Low	23

*Gain according to the design model. +Calculated FoM does not include voltage.

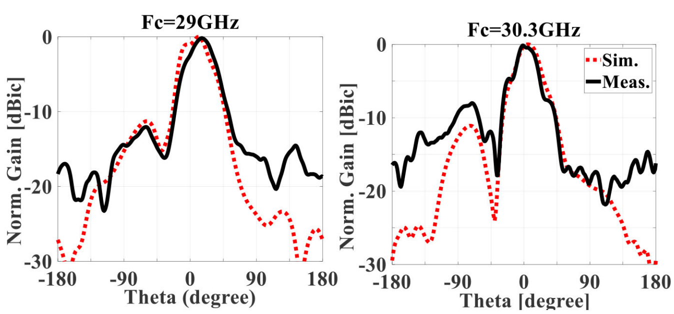

Fig. 7. Simulated and measured radiation patterns of the reconfigurable filtenna array at $\Phi = 90°$ for the ON state -29 GHz and OFF state -30.3 GHz.

The comparison between the simulated and measured input reflection coefficient of the filtenna is shown in Fig. 6(c). The measured results match the predicted simulated ones for both states of the active filtenna. The actual operating bandwidths for the two states of the system are 29.65–30.8 and 28.55–29.65 GHz, respectively. The reflection coefficient of the array alone is also presented in Fig. 6(c). Such response proves that the filtenna structure is able to provide the required filtering functionality by following the mode of operation of the integrated BPF. Fig. 6(d) depicts the realized gain of the antenna system. The minimum and maximum CP gains (at $\Theta = 0^{\circ}$) for the lower and upper bands are 8.4–10.4 and 10.3–11 dBic, respectively. Again, the measured gain of the filtenna agrees with the simulated data. The AR of the antenna at $\Theta = 0°$ is shown in Fig. 6(e), which ensures CP for both operating states of the p-i-n diode. The measured AR performs similarly to the simulated results. The proposed filtenna structure is able to provide circularly polarized radiation with a gain beyond 9 dBic for the frequency range 28.75–30.55 GHz at the two states of the integrated p-i-n diode. The simulated and measured filtenna's radiation efficiency for both states of the p-i-n diode is presented in Fig. 6(f). The filtenna prototype is able to produce efficiency of more than 70% across the two reconfigurable frequency bands.

Moreover, the two-band active filtenna structure characterization is concluded with the normalized radiation pattern plots of Fig. 7. The patterns' measurements are taken for the two center frequencies of the system, (29 and 30.3 GHz) at the $\Phi = 90^{\circ}$. The sidelobe level (SLL) for the ON and OFF states is -12 and -8 dB, respectively. The noticed discrepancies in the back lobes are attributed to the coupling effect on the copper wires serving for the dc supply of the p-i-n diode. The measured patterns are also well predicted by the simulated ones.

Table I compares the proposed reconfigurable filtenna structure with other work in the literature. An FoM is defined as presented in (1). The FoM is derived by accounting for the number of reconfigurable bands (`#Rec.band`), the peak gain (`Gain`), the voltage required to activate the two frequency bands (`Voltage`), and the number of layers (`#layers`) utilized for the antenna fabrication. The FoM also accounts for the fabrication complexity and cost (`Cost-Complexity`) with an assigned weight of 1 (for low-complex structures) and 2 (for high-complex structures). The superior performance of the proposed design in this letter is exhibited with the highest value of the FoM (i.e., 23) in comparison with the other reported work in the literature. Such FoM demonstrates the superior behavior of the presented filtenna structure in providing a high-gain circularly polarized radiation with frequency reconfiguration over two distinct operating bandwidths within the Ka-band

$$\mathrm{FOM} = \frac{\#\mathrm{Rec.\,Band} \times \mathrm{Gain}}{\mathrm{Voltage} \times \#\mathrm{Layers} \times \mathrm{Cost} - \mathrm{Complexity}}. \quad (1)$$

V. CONCLUSION

This letter introduces a new compact active filtenna for CubeSats that covers the frequency range of 28.55–30.85 GHz. The circularly polarized array is reconfigured through a tunable BPF resulting in a reconfigurable filtenna. The proposed filtenna consists of a wideband RHCP four-element antenna array fed by a sequentially rotated feeding network and driven by the modified ring resonator BPF. The ring resonator employs a loaded reactance in the form of an open stub, which is reconfigured by relying on a p-i-n diode. The fabricated prototype exhibits for the two reconfigurable states a reflection coefficient less than -15 dB, realized gain at the two center frequencies greater than 10 dBic, an AR less than 1 dB, and a directional pattern with SLL less than -8 dB. The presented filtenna constitutes a unique contribution to reconfigurable antennas at the Ka-band by exhibiting frequency reconfiguration, with high CP purity while relying on a single p-i-n diode.

REFERENCES

[1] J. Alvarez and B. Walls, “Constellations, clusters, and communication technology: Expanding small satellite access to space,” in *Proc. IEEE Aerosp. Conf.*, 2016, pp. 1–11.

[2] S. Gao *et al.*, “Antennas for modern small satellites,” *IEEE Antennas Propag. Mag.*, vol. 51, no. 4, pp. 40–56, Aug. 2009.

[3] N. Chahat, *CubeSat Antenna Design*. Hoboken, NJ, USA: Wiley, 2021.

[4] J. Costantine, Y. Tawk, S. E. Barbin, and C. G. Christodoulou, “Reconfigurable antennas: Design and applications,” *Proc. IEEE*, vol. 103, no. 3, pp. 424–437, Mar. 2015.

[5] M. Alibakhshikenari, B. S. Virdee, C. H. See, R. A. Abd-Alhameed, F. Falcone, and E. Limiti, “High-gain metasurface in polyimide on-chip antenna based on CRLH-TL for sub-terahertz integrated circuits,” *Sci. Rep.*, vol. 10, no. 1, 2020, Art. no. 4298.

[6] M. Alibakhshikenari *et al.*, “Study on improvement of the performance parameters of a novel 0.41–0.47 THz on-chip antenna based on metasurface concept realized on 50 μm GaAs-layer,” *Sci. Rep.*, vol. 10, no. 1, 2020, Art. no. 11034.

[7] M. Alibakhshikenari *et al.*, “Study on on-chip antenna design based on metamaterial-inspired and substrate-integrated waveguide properties for millimetre-wave and THz integrated-circuit applications,” *J. Infrared, Millimeter, Terahertz Waves*, vol. 42, no. 1, pp. 17–28, 2021.

[8] M. S. Anwar and A. Bangert, “Broadband frequency reconfigurable antenna using capacitive loading for K-band applications,” in *Proc. 14th Eur. Conf. Antennas Propag.*, Copenhagen, Denmark, 2020, pp. 1–5.

[9] J. Kim and J. Oh, “Liquid-crystal-embedded aperture-coupled microstrip antenna for 5G applications,” *IEEE Antennas Wireless Propag. Lett.*, vol. 19, no. 11, pp. 1958–1962, Nov. 2020.

[10] I. F. da Costa, A. Cerqueira S., D. H. Spadoti, L. G. da Silva, J. A. J. Ribeiro, and S. E. Barbin, “Optically controlled reconfigurable antenna array for mm-wave applications,” *IEEE Antennas Wireless Propag. Lett.*, vol. 16, pp. 2142–2145, 2017.

[11] L. Li *et al.*, “Frequency-reconfigurable quasi-Sierpinski antenna integrating with dual-band high-impedance surface,” *IEEE Trans. Antennas Propag.*, vol. 62, no. 9, pp. 4459–4467, Sep. 2014.

[12] Y. Tawk, J. Costantine, and C. G. Christodoulou, “Reconfigurable filtennas and MIMO in cognitive radio applications,” *IEEE Trans. Antennas Propag.*, vol. 62, no. 3, pp. 1074–1083, Mar. 2014.

[13] J. Deng, S. Hou, L. Zhao, and L. Guo, “A reconfigurable filtering antenna with integrated bandpass filters for UWB/WLAN applications,” *IEEE Trans. Antennas Propag.*, vol. 66, no. 1, pp. 401–404, Jan. 2018.

[14] H. A. Atallah, A. B. Abdel-Rahman, K. Yoshitomi, and R. K. Pokharel, “Compact frequency reconfigurable filtennas using varactor loaded T-shaped and H-shaped resonators for cognitive radio applications,” *Microw. Antennas Propag.*, vol. 10, no. 9, pp. 991–1001, 2016.

[15] A. H. Ramadan, J. Costantine, M. Al-Husseini, M. Mervat, Y. Tawk, and C. Christodoulou, “Tunable filter-antennas for cognitive radio applications,” *Prog. Electromagn. Res.*, vol. 57, pp. 253–265, 2014.

[16] H.-Y. Li, C.-T. Yeh, J.-J. Huang, C.-W. Chang, C.-T. Yu, and J.-S. Fu, “CPW-fed frequency-reconfigurable slot-loop antenna with a tunable matching network based on ferroelectric varactors,” *IEEE Antennas Wireless Propag. Lett.*, vol. 14, pp. 614–617, 2015.

[17] J. Choi *et al.*, “Frequency-adjustable planar folded slot antenna using fully integrated multithrow function for 5G mobile devices at millimeter-wave spectrum,” *IEEE Trans. Microw. Theory Techn.*, vol. 68, no. 5, pp. 1872–1881, May 2020.

[18] B. Rohrdantz, V. Schmidt, and A. F. Jacob, “Microstrip ring resonator based frequency reconfigurable band-pass filters at K-band,” in *Proc. 20th Int. Conf. Microw., Radar Wireless Commun.*, 2014, pp. 1–4.

[19] M. Patriotis, F. N. Ayoub, and C. G. Christodoulou, “A Ka-band frequency reconfigurable circularly polarized antenna array using a ring resonator,” in *Proc. IEEE Int. Symp. Antennas Propag. USNC/URSI Nat. Radio Sci. Meeting*, Boston, MA, USA, 2018, pp. 467–468.

[20] B. Lee and Y. Yoon, “Low-profile, low-cost, broadband millimeter-wave antenna array for high-data-rate WPAN systems,” *IEEE Antennas Wireless Propag. Lett.*, vol. 16, pp. 1957–1960, 2017.

[21] A. Chen, Y. Zhang, Z. Chen, and C. Yang, “Development of a Ka-band wideband circularly polarized 64-element microstrip antenna array with double application of the sequential rotation feeding technique,” *IEEE Antennas Wireless Propag. Lett.*, vol. 10, pp. 1270–1273, 2011.

[22] “AlGaAs Flip Chip PIN diodes,” *Datasheet MA4AGP907*, M/A-COM Technology Solutions Inc., (MACOM), Lowel, Massachusetts, United States of America, 2020. [Online]. Available: https://cdn.macom.com/datasheets/MA4AGP907__MA4AGFCP910.pdf

[23] K. van Caekenberghe and K. Sarabandi, “A 2-bit Ka-band RF MEMS frequency tunable slot antenna,” *IEEE Antennas Wireless Propag. Lett.*, vol. 7, pp. 179–182, 2008.

[24] B. Ghassemiparvin and N. Ghalichechian, “Paraffin-based reconfigurable antenna operating at 100 GHz,” *J. Microelectromech. Syst.*, vol. 29, no. 5, pp. 621–628, 2020.